ACUSTICA · acta acustica
Vol. 82 (1996) 829–838

Theoretical Study of the Stoneley-Scholte Wave at the Interface between an Ideal Fluid and a Viscoelastic Solid

N. Favretto-Anrès

Centre National de la Recherche Scientifique, Laboratoire de Mécanique et d'Acoustique, Équipe Acoustique Sous-Marine et Modélisation, 31 chemin J. Aiguier, 13402 Marçeille Cedex 20, France

Summary

The propagation of the Stoneley-Scholte wave is analysed at the boundary between an ideal fluid and a viscoelastic solid. The theoretical study is developed using the approach of the inhomogeneous plane waves: the interface wave is thus regarded as a linear combination of one evanescent wave in the fluid and two heterogeneous waves in the solid. The main interest of the paper is the introduction of the viscoelastic solid, which is a medium characterized by physical attenuation, in the study of the propagation of the interface wave. Its mechanical viscosities are expressed in terms of acoustical attenuations, more easily determined by means of acoustical measurements. Existing mathematical tools are then used for solving the dispersion equation determined in this case. The study presented in the paper deals only with some aspects of the direct problem, that is the determination of the propagation properties of the Stoneley-Scholte wave, established for two different interfaces. A comparison of these characteristics in the presence and in the absence of attenuation, and a parametric study of the effect of attenuation, are included. The validity of the theoretical results are finally well demonstrated with some experimental ones, obtained with synthetic resins modelling viscoelastic solids.

PACS no. 43.30.Ma, 43.20.Gp

1. Introduction

The sea bed is generally composed of marine sediments lying on a rocky elastic base. The sediments are layered media resulting from many complex processes (erosion, deposits, ...). The acoustical recognition of the bottom, which interests marine geologists, oil and fishing industries and military institutions, is then impossible without coring or acoustical probing. Techniques using coring do not allow us to accurately determine the shear wave velocity of the sediments, whose knowledge would lead to information about the grain size distribution of the sediments (Le Tirant, 1976). So far, for the geoacoustical characterization of the sea bed, measuring its reflection coefficient is the most used technique in the acoustical field. This measurement leads to the determination of the longitudinal wave velocities and the densities of the layers, whose nature can then be identified (Bjørnø *et al.*, 1994), and sometimes to the determination of the shear wave velocities (Chapman *et al.*, 1986). Some methods, based on analysis of the Stoneley-Scholte wave, are also under consideration for the acoustical characterization of the first layer of the sea floor (Caiti *et al.*, 1991; Guilbot, 1994). Indeed the wave is sensitive to the shear wave velocity of the solid medium. But few works are concerned with the determination of the shear wave attenuation of the sedimentary layer. The only ones just treat the numerical modelling of the interface wave data (Jensen and Schmidt, 1986).

The aim of the paper is the theoretical study of the propagation of the Stoneley-Scholte wave, at the plane boundary between water and a viscoelastic solid. Plane wave geometry was assumed and the study was based on the consideration of inhomogeneous plane wave propagation in both media. The Stoneley-Scholte wave was then locally regarded as a linear combination of one evanescent plane wave in the fluid and two heterogeneous plane waves in the solid. The description of these inhomogeneous waves is shown in Table I (Poirée, 1991). The propagation and the attenuation of the homogeneous waves are described by means of a complex-valued wavenumber, whereas those of the inhomogeneous waves are represented by means of a complex-valued wave vector. The evanescent waves, whose propagation vector is at right angles to the attenuation vector, is a special case of the heterogeneous waves. The advantage of such a representation is a good description of the wave propagation geometry, and then a better understanding of the problem. The most interesting aspect of this work is the treatment of the viscoelastic solid for studies of the interface wave propagation: the solid medium was characterized by physical attenuation. The study presented in the paper deals only with some aspects of the direct problem, that is the determination of the propagation characteristics. But it can be viewed as a first step towards the recovery of the shear wave parameters of solid materials (velocity and attenuation), using measurements of the interface waves, propagating at the boundary between a fluid and a solid. Such an approach can then be used in underwater acoustics for the identification of the sea bottom, and in particular for the identification of the sedimentary layer.

The sediments, which are viscoelastic, were represented by the Kelvin-Voigt model. The viscosity coefficients, introduced in the constitutive law of the solid, could not be determined mechanically for frequencies higher than 10 kHz. But the attenuations of the homogeneous waves propagating in the solid material could be easily determined by means of acoustical measurements. A relation between the viscosity coefficients and the attenuations is then established in section 2. Section 3 is concerned with some theoretical reminds on the properties of the inhomogeneous waves (heteroge-

Received 12 October 1994,
accepted 17 January 1996.

ACUSTICA · acta acustica
Vol. 82 (1996)

Table I. Classification of the different harmonic plane waves (k': propagation wavenumber, k'': attenuation wavenumber, $\boldsymbol{K}'$: propagation vector, $\boldsymbol{K}''$: attenuation vector.

Homogenous plane waves		Inhomogenous plane waves	
Undamped	Damped	Evanescent	Heterogenous
k'	k' k''	$\boldsymbol{K}''$ $\theta = 90°$ $\boldsymbol{K}'$	$\boldsymbol{K}''$ $0 < \theta < 90°$ $\boldsymbol{K}'$

neous and evanescent ones). Section 4 is devoted to study of the propagation of the Stoneley-Scholte wave at the ideal fluid/viscoelastic solid interface, and the properties of the interface wave are described. Two examples of the fluid/solid configuration illustrate the theoretical results and a comparison of these characteristics in the presence and in the absence of attenuation, and a parametric study of the effect of attenuation, are included. Finally, in section 5, some experimental results, obtained with synthetic resins modelling sediments, demonstrate the validity of the theoretical ones.

2. Damped homogeneous plane waves in a viscoelastic solid – Relation with the viscosity coefficients

The marine sedimentary bottom is attenuating. In order to accurately compare seismic data and the experimental results obtained with models of sediments in laboratory, the sediment behavior was modelled on a viscoelastic behavior. In our laboratory, the sediments are generally modelled on synthetic resins, which have the same acoustical properties (Rabau, 1990). The velocities of the homogeneous plane waves in these materials have been acoustically measured, and they are almost constant in the used frequency range 100 kHz–5 MHz. We assumed that they were also constant for frequencies greater than 20 kHz and less than 100 kHz. The behavior of the viscoelastic solid could not be described by means of the Kramers-Krönig relations or classical equations of viscoelasticity, using Laplace-Carson transforms. These two methods, which allow us to obtain the velocity in terms of the attenuation in the whole frequency domain, became ineffective in our case, because the parameters of the solid were constant in the used frequency range. Modelling the sediments on the generalized Kelvin-Voigt model (parallel connection between springs and dashpots) would be also certainly rigorous, but the problem would quickly become very complicated, because there would be as many unknowns as introduced elements. Therefore, the solid was represented by the Kelvin-Voigt model, which is more ordinary.

The viscosity coefficients λ' and μ' introduced in the constitutive law of the solid, could not be obtained from mechanical measurements in the high frequency range of our interest. Therefore, a relation was established with the attenuations of the homogeneous plane waves. The advantage of such a modelling respect to the previous ones is, on one hand, to be ordinary and quite rigorous for describing the properties of the solid in the theory of the propagation of the interface waves. On the other hand, the attenuation of the homogeneous waves in the solid can be easily determined by means of acoustical measurements. Finally, we can study theoretically the propagation of the interface wave, but keeping in our mind the experiments on the attenuation.

2.1. Equations of propagation

We approach the behavior of the isotropic viscoelastic solid by the Kelvin-Voigt model. The model represents a parallel connection between a spring (elasticity), and a dashpot (linear viscosity). It corresponds to a decomposition of the stress tensor in an elastic stress tensor $\boldsymbol{\sigma}_e$, and an unelastic stress tensor $\boldsymbol{\sigma}_v$. The latter characterizes the intrinsic phenomenon of the viscosity of the solid material (Lemaître and Chaboche, 1985):

$$\boldsymbol{\sigma} = f(\boldsymbol{\varepsilon}, \dot{\boldsymbol{\varepsilon}}) = \boldsymbol{\sigma}_e + \boldsymbol{\sigma}_v \tag{1}$$

where $\boldsymbol{\varepsilon} = \frac{1}{2}(\mathrm{grad}\boldsymbol{\xi} + (\mathrm{grad}\boldsymbol{\xi})^t)$ is the strain tensor, $\dot{\boldsymbol{\varepsilon}}$ the tensor derived with respect to time (strain velocity tensor) and $\boldsymbol{\xi}$ the displacement vector. Isotropic and linear elasticity implies similar relations for both stress tensors $\boldsymbol{\sigma}_e$ and $\boldsymbol{\sigma}_v$ (case of plane strains $\varepsilon_{33} = \varepsilon_{13} = \varepsilon_{23} = 0$) (Salençon, 1983):

$$\boldsymbol{\sigma}_e(t) = 2\mu(t) * \boldsymbol{\varepsilon}(t) + \lambda(t) * \big(Tr\,\boldsymbol{\varepsilon}(t)\big)\boldsymbol{I} \tag{2}$$

$$\boldsymbol{\sigma}_v(t) = 2\mu'(t) * \dot{\boldsymbol{\varepsilon}}(t) + \lambda'(t) * \big(Tr\,\dot{\boldsymbol{\varepsilon}}(t)\big)\boldsymbol{I} \tag{3}$$

where λ and μ are the elasticity coefficients, λ' and μ' the viscosity coefficients (Deschamps, 1991), $\boldsymbol{I}$ the unit matrix and the asterisk $*$ indicates the convolution. These relations are derived from the generalization of the Hooke law.

The linearized dynamic equation assuming small perturbations, which is referred to the undamped condition (without viscosity), gave the equation of propagation in terms of displacement $\boldsymbol{\xi}$:

$$\begin{aligned}\rho\frac{\partial^2\boldsymbol{\xi}(\boldsymbol{r},t)}{\partial t^2} &+ \mu(t) * \mathrm{rot}\ \mathrm{rot}\,\boldsymbol{\xi}(\boldsymbol{r},t) \\ &- \big(2\mu(t) + \lambda(t)\big) * \mathrm{grad}\,\mathrm{div}\,\boldsymbol{\xi}(\boldsymbol{r},t) \\ &+ \mu'(t) * \mathrm{rot}\,\mathrm{rot}\,\frac{\partial\boldsymbol{\xi}(\boldsymbol{r},t)}{\partial t} \\ &- \big(2\mu'(t) + \lambda'(t)\big) * \mathrm{grad}\,\mathrm{div}\,\frac{\partial\boldsymbol{\xi}(\boldsymbol{r},t)}{\partial t} = 0\end{aligned} \tag{4}$$

where ρ was the density of the solid and $\boldsymbol{r}$ the space vector. The expression of the displacement for the harmonic waves was assumed to be as follows:

$$\boldsymbol{\xi}(\boldsymbol{r},t) = \boldsymbol{\zeta}(\boldsymbol{r})\,\mathrm{e}^{-\mathrm{i}\,\omega t}. \tag{5}$$

After simplification, the equation of propagation was written as:

$$\begin{aligned}\rho\omega^2\boldsymbol{\zeta}(\boldsymbol{r}) &+ \Big[\big(2M(\omega) + \Lambda(\omega)\big) \\ &\quad - \mathrm{i}\omega\big(2M'(\omega) + \Lambda'(\omega)\big)\Big]\mathrm{grad}\,\mathrm{div}\,\boldsymbol{\zeta}(\boldsymbol{r}) \\ &- \Big[M(\omega) - \mathrm{i}M'(\omega)\Big]\mathrm{rot}\,\mathrm{rot}\,\boldsymbol{\zeta}(\boldsymbol{r}) = 0\end{aligned} \tag{6}$$

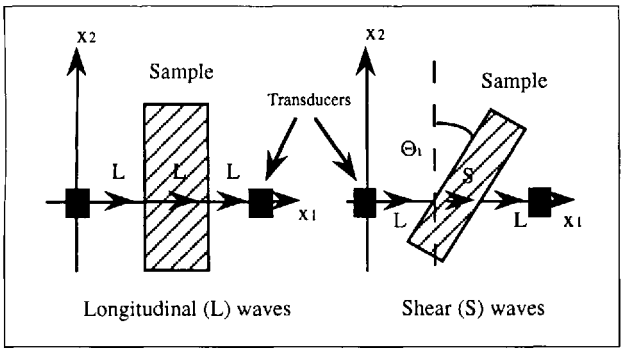

Figure 1. Geometry used for the measurements of the attenuations of the longitudinal and shear waves in a solid material.

where $M(\omega)$ and $\Lambda(\omega)$ were the Fourier transforms of $\mu(t)$ and $\lambda(t)$, and $M'(\omega)$ and $\Lambda'(\omega)$ the Fourier transforms of $\mu'(t)$ and $\lambda'(t)$.

2.2. Irrotational and solenoidal solutions

The displacement ζ could be decomposed in two displacements ζ_l and ζ_t, which respectively corresponded to the irrotational waves ($\mathrm{rot}\zeta_l = 0$) and the solenoidal waves ($\mathrm{div}\,\zeta_t = 0$). We set $\nu_l(\omega) = \frac{2M'+\Lambda'}{\rho c_l^2}$ and $\nu_t(\omega) = \frac{M'}{\rho c_t^2}$ were the ratio between the viscosity and Lamé coefficients. Equation (6) was thus written as:

$$\Delta\zeta_m\big(1 - \mathrm{i}\omega\,\nu_m(\omega)\big) + k_m^2\zeta_m = 0, \tag{7}$$

where k_m was the wave number of the irrotational ($m \sim l$) or solenoidal waves ($m \sim t$).

In the case where the inequality $\omega\nu_m(\omega) \ll 1$ was verified, we could use the first order approximation of equation (7):

$$\Delta\zeta_m + k_m^2\big(1 + \mathrm{i}\omega\,\nu_m\big)\zeta_m = 0. \tag{8}$$

The assumptions $\omega\nu_m \ll 1$ ($m \sim l$ or $m \sim t$), which express the viscosity constants in terms of the density and the homogeneous waves velocities in the solid material, are always verified for the materials (synthetic resins) we use to model the sedimentary bottom, in our used frequency range. One can reasonably think that this inequality is also verified for real sediments and the low frequency range of the in situ measurements.

2.3. Damped longitudinal and shear plane waves

Experimentally, one always measures the longitudinal and shear wave attenuations along their propagation direction x_1 through the solid material, as it is shown on Figure 1. Thus, the vector ζ_m was written as:

$$\zeta_m = \zeta_{0m}\,\mathrm{e}^{\mathrm{i}K_m^* x_1}x_1, \tag{9}$$

$$K_m^{*\,2} = k_m^2 + \mathrm{i}\omega\,\nu_m k_m^2, \tag{10}$$

where K_m^* was the complex wave number of the damped homogeneous plane waves in the solid, and ζ_{0m} a constant.

Setting $K_m^{*\,2} = (K_m' + \mathrm{i}K_m'')^2$, and comparing the real and imaginary parts of the equality with those of equation (10), we obtained a system of two equations in the two unknowns K_m' and K_m'' for each kind of the homogeneous waves:

$$K_m'^{\,2} - K_m''^{\,2} = k_m^2, \tag{11}$$

$$K_m' K_m'' = \frac{1}{2}\omega\nu_m k_m^2. \tag{12}$$

This system could be easily solved due to the assumption $\omega\nu_m \ll 1$, and finally, the displacement vector could be written as:

$$\zeta_m = \zeta_{0m}\,\mathrm{e}^{-\frac{1}{2}\omega\nu_m k_m x_1}\,\mathrm{e}^{\mathrm{i}k_m x_1}x_1. \tag{13}$$

The first exponent corresponds to the wave attenuation and the second one to the wave propagation.

The difference with the undamped condition (the left hand member of equation (12) is zero) concerns the nature of the attenuation expression. In the undamped case, the attenuation is spatial and is referred to the methematical representation of the wave, and not to the physical property of the solid material. In the damped case, the attenuation both describes the representation of the wave and the viscoelasticity of the solid.

2.4. Relation to experiments

The solids, used for modelling the sedimentary bottom, are attenuating. And the wave is often completely attenuated before doing one full return inside the solid. Performing accurate measurements of the attenuations then requires two solid samples with reasonable thicknesses. Then, for a given frequency, the experimental coefficient α ($\alpha < 0$) of the attenuation, expressed in Nepers per meter, is given by the espression:

$$\alpha = \frac{\ln(A_1/A_2)}{e_1 - e_2} \tag{14}$$

that is:

$$\frac{A_1}{A_2} = \mathrm{e}^{\alpha(e_1 - e_2)}, \tag{15}$$

where A_1 and A_2 are the amplitudes of the signals, received through two solid samples of thicknesses e_1 and e_2.

Comparing equation (13) and equation (15) enabled us to relate the viscosity coefficients Λ' and M' to the acoustical attenuations α_l and α_t of the longitudinal and shear waves, for a given frequency:

$$\big|\alpha_m(\omega)\big| = \frac{1}{2}k_m\omega\nu_m(\omega), \tag{16}$$

that was, substituting ν_m for their expression:

$$\Lambda' = \frac{2\rho}{\omega^2}\Big(\big|\alpha_l(\omega)\big|c_l^3 - 2\big|\alpha_t(\omega)\big|c_t^3\Big), \tag{17}$$

$$M' = \frac{2\rho}{\omega^2}\big|\alpha_t(\omega)\big|c_t^3. \tag{18}$$

Defining the viscosity coefficients in the whole frequency range leads to perform the measurements of the acoustical attenuations for each frequency, or to know the behavior of the attenuation curves.

ACUSTICA · acta acustica
Vol. 82 (1996)

3. Recall of some properties of the inhomogeneous plane waves

3.1. In a solid medium

In linear acoustics, the equation of propagation in a solid medium, supposed to be perfectly elastic, homogeneous, isotropic and infinite, is written as:

$$\rho\frac{\partial^2\boldsymbol{\xi}_S(\boldsymbol{r},t)}{\partial t^2} - \mu(t) * \operatorname{div}\operatorname{grad}\boldsymbol{\xi}_S(\boldsymbol{r},t) - \big(\lambda(t)+\mu(t)\big) * \operatorname{grad}\operatorname{div}\boldsymbol{\xi}_S(\boldsymbol{r},t) = 0 \tag{19}$$

or

$$\rho\frac{\partial^2\boldsymbol{\xi}_S(\boldsymbol{r},t)}{\partial t^2} + \mu(t) * \operatorname{rot}\operatorname{rot}\boldsymbol{\xi}_S(\boldsymbol{r},t) - \big(2\mu(t)+\lambda(t)\big) * \operatorname{grad}\operatorname{div}\boldsymbol{\xi}_S(\boldsymbol{r},t) = 0. \tag{20}$$

ρ is the solid density, λ and μ the Lamé coefficients, $\boldsymbol{\xi}_S$ the displacement vector and $\boldsymbol{r}$ the space vector.

For the harmonic plane waves with the angular frequency ω, the expression of the displacement was assumed to be as follows:

$$\boldsymbol{\xi}_S(\boldsymbol{r},t) = \boldsymbol{\zeta}_S(\boldsymbol{r})\,\mathrm{e}^{-\mathrm{i}\,\omega t}, \tag{21}$$

and the equation of propagation was written as:

$$\rho\omega^2\boldsymbol{\zeta}_S(\boldsymbol{r}) + \big(2M(\omega)+\Lambda(\omega)\big)\operatorname{grad}\operatorname{div}\boldsymbol{\zeta}_S(\boldsymbol{r}) - M(\omega)\operatorname{rot}\operatorname{rot}\boldsymbol{\zeta}_S(\boldsymbol{r}) = 0, \tag{22}$$

where $M(\omega)$ and $\Lambda(\omega)$ were the Fourier transforms of $\mu(t)$ and $\lambda(t)$.

The real-valued displacement vector $\boldsymbol{\zeta}_S$ in the solid could be regarded as the sum of two real-valued displacement vectors (Poirée, 1989), corresponding to the *lamellar* displacement $\boldsymbol{\zeta}_L$ and to the *torsional* displacement $\boldsymbol{\zeta}_T$:

$$\boldsymbol{\zeta}_S = \boldsymbol{\zeta}_L + \boldsymbol{\zeta}_T \tag{23}$$

$$\operatorname{rot}\boldsymbol{\zeta}_L = 0 \tag{24}$$

$$\operatorname{div}\boldsymbol{\zeta}_T = 0. \tag{25}$$

The acoustic real-valued displacements $\boldsymbol{\zeta}_L$ and $\boldsymbol{\zeta}_T$ were given from the complex-valued displacement vector $\boldsymbol{\zeta}^*_M$:

$$\boldsymbol{\zeta}_L = \Re e\{\boldsymbol{\zeta}^*_L\}, \qquad \boldsymbol{\zeta}_T = \Re e\{\boldsymbol{\zeta}^*_T\} \tag{26}$$

$$\boldsymbol{\zeta}^*_M = \boldsymbol{\zeta}^{*0}_M\,\mathrm{e}^{\,\mathrm{i}\,\boldsymbol{K}^*_M\cdot\boldsymbol{r}}. \tag{27}$$

The subscript $M{=}L,T$ was used to denote the lamellar and torsional waves. $\boldsymbol{\zeta}^{*0}_M$ was a complex-valued constant vector and K^*_M the complex-valued wave vector of the inhomogeneous waves.

The complex-valued wave vector of the inhomogeneous waves was written in the following way:

$$\boldsymbol{K}^*_M = \boldsymbol{K}'_M + \mathrm{i}\boldsymbol{K}''_M. \tag{28}$$

The real-valued vectors $\boldsymbol{K}'_M$ and $\boldsymbol{K}''_M$ respectively represent the *propagation* and the *attenuation* of the wave. Notice that the attenuation is due to the spatial structure of the wave, and not to the nature of the solid material.

From equation (22), the wave vectors of the evanescent plane waves (lamellar and torsional) were connected to the wave numbers of the associated homogeneous plane waves (longitudinal ($m \sim t$) and shear ($m \sim t$) ones) by:

$$\boldsymbol{K}^*_M \cdot \boldsymbol{K}^*_M = k^2_m, \tag{29}$$

that was:

$$\boldsymbol{K}'^{\,2}_M - \boldsymbol{K}''^{\,2}_M = k^2_m, \tag{30}$$

$$\boldsymbol{K}'_M \cdot \boldsymbol{K}''_M = 0 \quad\Rightarrow\quad \boldsymbol{K}'_M \perp \boldsymbol{K}''_M. \tag{31}$$

The quantities $k_l = \frac{\omega}{c_l}$ and $c^2_l = \frac{\Lambda+2M}{\rho}$ defined the longitudinal wave number and velocity, $k_t = \frac{\omega}{c_t}$ and $c^2_t = \frac{M}{\rho}$ the shear wave number and velocity.

Equation (30) suggests that the velocity of the inhomogeneous waves is less than the velocity of the associated homogeneous waves:

$$c_M = \frac{\omega}{K'_M} < c_m = \frac{\omega}{k_m}. \tag{32}$$

3.2. In a viscoelastic solid medium

The equation of propagation in a solid medium, supposed to be viscoelastic, homogeneous, isotropic and infinite was expressed by equation (4). For the harmonic plane waves with the angular frequency ω, it could be written as equation (6). The displacement vectors of the heterogeneous waves in the solid were given by equation (23), (24), (25), (26), (27) and (28), where $\boldsymbol{K}^*_M$ was defined by:

$$\boldsymbol{K}^*_M \cdot \boldsymbol{K}^*_M = k^2_m(1+\mathrm{i}\,\omega\,\nu_m), \tag{33}$$

with $\nu_{(m\sim l)}(\omega) = \frac{2M'+\Lambda'}{\rho c^2_l}$ and $\nu_{(m\sim t)}(\omega) = \frac{M'}{\rho c^2_t}$, that was:

$$\boldsymbol{K}'^{\,2}_M - \boldsymbol{K}''^{\,2}_M = k^2_m, \tag{34}$$

$$\boldsymbol{K}'_M \cdot \boldsymbol{K}''_M = \frac{1}{2}\omega\nu_m k^2_m \tag{35}$$

$$\Rightarrow \cos\Theta_M = \frac{\omega\nu_m k^2_m}{2K'_M K''_M},$$

which defined the angle $\Theta_M = (\boldsymbol{K}'_M, \boldsymbol{K}''_M)$.

3.3. In an ideal fluid medium

The equation of propagation in an ideal fluid was written as:

$$\rho_0\frac{\partial^2\boldsymbol{\xi}_F(\boldsymbol{r},t)}{\partial t^2} - \lambda_0(t) * \operatorname{grad}\operatorname{div}\boldsymbol{\xi}_F(\boldsymbol{r},t) = 0. \tag{36}$$

ρ_0 is the fluid density, λ_0 the Lamé coefficient and $\boldsymbol{\xi}_F$ the displacement vector.

For the harmonic plane waves with the angular frequency ω, it could be written as:

$$\rho_0\omega^2\boldsymbol{\zeta}_F(\boldsymbol{r}) - \Lambda_0(\omega)\operatorname{grad}\operatorname{div}\boldsymbol{\zeta}_F(\boldsymbol{r}) = 0, \tag{37}$$

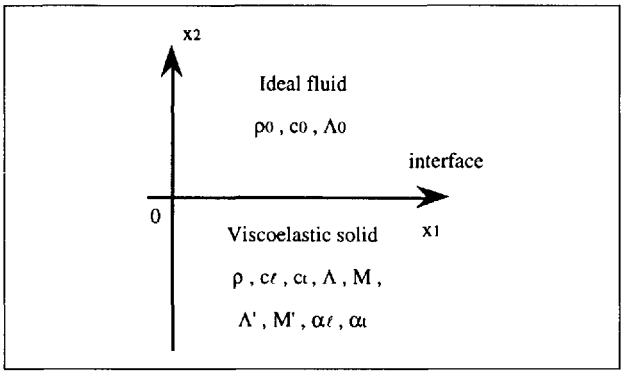

Figure 2. Ideal fluid/viscoelastic solid interface.

where $\Lambda_0(\omega)$ was the Fourier transform of $\lambda(t)$.

The real-valued displacement $\boldsymbol{\zeta}_F$ in the fluid, corresponding to a lamellar displacement ($\mathrm{rot}\,\boldsymbol{\zeta}_F = 0$) was described, from the complex-valued displacement $\boldsymbol{\zeta}_F^*$, by the equation:

$$\boldsymbol{\zeta}_F = \Re e\{\boldsymbol{\zeta}_F^*\}, \tag{38}$$

where

$$\boldsymbol{\zeta}_F^* = \boldsymbol{\zeta}_F^{*0}\, e^{i\boldsymbol{K}_F^*\cdot\boldsymbol{r}}, \tag{39}$$
$$\boldsymbol{K}_F^* = \boldsymbol{K}_F' + i\boldsymbol{K}_F'', \tag{40}$$
$$\boldsymbol{K}_F^* \cdot \boldsymbol{K}_F^* = k_0^2, \tag{41}$$

that was:

$$\boldsymbol{K}_F'^2 - \boldsymbol{K}_F''^2 = k_0^2, \tag{42}$$
$$\boldsymbol{K}_F' \cdot \boldsymbol{K}_F'' = 0. \tag{43}$$

The term $\boldsymbol{\zeta}_F^{*0}$ was a complex-valued constant vector, $\boldsymbol{K}_F^*$ the complex-valued wave vector of lamellar waves, $k_0 = \frac{\omega}{c_0}$ the wave number of the associated homogeneous waves and $c_0 = \frac{\lambda_0}{\rho_0}$ the longitudinal wave velocity.

4. The Stoneley-Scholte wave at the plane interface between an ideal fluid and a viscoelastic solid – Theoretical results and numerical application

The Stoneley-Scholte wave has been generally studied at the ideal fluid/solid interface. Poirée and Luppé have analysed it (Poirée and Luppé, 1991), seeking local solutions as linear combinations of evanescent plane waves, satisfying boundary conditions at the interface in both media. Few works have concerned with a non-ideal interface. Vol'kenshtein and Levin have investigated the structure of a Stoneley-Scholte wave at an interface between a viscous fluid and a solid (Vol'kenshtein and Levin, 1988). In the present study, the propagation of the Stonely-Scholte wave was analysed at the plane boundary between an ideal fluid, which modelled the sea, and a viscoelastic solid, which modelled the sediments (Figure 2). The interface wave was then locally represented in the from of a linear combination of three inhomogeneous waves (one evanescent wave in the fluid and two heterogeneous waves in the solid).

4.1. Fundamentals

The displacement of the lamellar evanescent wave in the fluid and those of the lamellar and torsional heterogeneous waves in the viscoelastic solid are described in section 3.

The projections $\boldsymbol{K}_{M1}^*$ and $\boldsymbol{K}_{M2}^*$ of the different vectors $\boldsymbol{K}_M^*$ upon the axis $\boldsymbol{x}_1$ and $\boldsymbol{x}_2$ verified several relations. First of all, Snell's law implied that the projections of the wave vectors upon the axis $\boldsymbol{x}_1$ were equal:

$$\boldsymbol{K}_{F1}^* = \boldsymbol{K}_{L1}^* = \boldsymbol{K}_{T1}^* = \boldsymbol{K}_1^*. \tag{44}$$

Therefore, this relation implied the equality of the real parts (propagation) of the projections of the wave vectors upon x_1, and also the equality of their imaginary parts (attenuation).

Next, lamellar and torsional waves in the solid had to fulfill the conditions deduced from equations (24) and (25):

$$K_1^*\zeta_{L2}^{*0} = K_{L2}^*\zeta_{L1}^{*0}, \tag{45}$$
$$K_1^*\zeta_{F2}^{*0} = K_{F2}^*\zeta_{F1}^{*0}, \tag{46}$$
$$K_1^*\zeta_{T1}^{*0} = -K_{T2}^*\zeta_{T2}^{*0}. \tag{47}$$

Finally, equations (33) and (41) became:

$$\boldsymbol{K}_1^{*2} + \boldsymbol{K}_{M2}^{*\,2} = k_m^2(1 + i\omega\nu_m), \tag{48}$$
$$\boldsymbol{K}_1^{*2} + \boldsymbol{K}_{F2}^{*\,2} = k_0^2. \tag{49}$$

At the ideal fluid/viscoelastic solid interface, normal stresses and displacements are continuous, and tangential stress in the solid is zero (Ewing *et al.*, 1957). If stresses were expressed in terms of displacements, one obtained from equations (45), (46) and (47) a system of three equations in the three unknowns $\zeta_{L2}^{*0}, \zeta_{T2}^{*0}, \zeta_{F2}^{*0}$:

$$\zeta_{L2}^{*0} + \zeta_{T2}^{*0} - \zeta_{F2}^{*0} = 0, \tag{50}$$
$$(AK_{L2}^{*2} + BK_1^{*2})\zeta_{L2}^{*0} + (A - B)K_{L2}^*K_{T2}^*\zeta_{T2}^{*0} - \frac{\rho_0}{\rho}\frac{K_{L2}^*}{K_{F2}^*}\omega^2\zeta_{F2}^{*0} = 0, \tag{51}$$
$$2K_1^{*2}\zeta_{L2}^{*0} + (K_1^{*2} - K_{T2}^{*2})\zeta_{T2}^{*0} = 0, \tag{52}$$

where

$$A = c_l^2(1 - i\omega\nu_l) \tag{53}$$
$$B = (c_l^2 - 2c_t^2)(1 - i\omega\nu_\theta) \tag{54}$$
$$\nu_\theta = 2\frac{|\alpha_l|c_l^3 - 2|\alpha_t|c_t^3}{\omega^2(c_l^2 - 2c_t^2)}. \tag{55}$$

4.2. The equation of dispersion and its numerical solution

Equating the determinant of the system to zero led to the characteristic equation of the Stoneley-Scholte wave in the unknown $\boldsymbol{K}_1^*$:

$$(K_1^{*2} - K_{T2}^{*2})W + 2K_1^{*2}K_{L2}^*K_{T2}^*X = \frac{\rho_0}{\rho}\frac{K_{L2}^*}{K_{F2}^*}k_t^4(1 - i\omega\nu_t), \tag{56}$$

ACUSTICA · acta acustica
Vol. 82 (1996)

with:

$$W = 2K_1^{*2}(1 - \mathrm{i}\,\omega\,\nu_\theta) + \mathrm{i}\omega\frac{c_l^2}{c_t^2}(\nu_l K_{L2}^{*2} - \nu_\theta K_1^{*2}) - Y, \quad (57)$$

$$Y = k_t^2(1 + \mathrm{i}\,\omega\,\nu_l), \quad (58)$$

$$X = 2(1 - \mathrm{i}\,\omega\,\nu_\theta) + \mathrm{i}\omega\frac{c_l^2}{c_t^2}(\nu_\theta - \nu_l). \quad (59)$$

Notice that, if the attenuation of the solid material was neglected, the equation became:

$$(K_1^{*2} - K_{T2}^{*2})^2 + 4K_1^{*2}K_{L2}^* K_{T2}^* = \frac{\rho_0}{\rho}\frac{K_{L2}^*}{K_{F2}^*}k_t^4. \quad (60)$$

It corresponds to the characteristic equation of the "classical" Stoneley-Scholte wave (Luppé, 1987), propagating along the ideal fluid/solid interface.

The solution of equation (56) in the complex plane K_1^* gave the Stoneley-Scholte wave velocity and attenuation, for a given frequency. The equation could not be analytically solved using the method of small perturbations, because the interface wave velocity was very different from the longitudinal wave velocity in the fluid or the shear wave velocity in the solid. This fact is due to the nature of the solid material.

Therefore, we used a numerical method which determines the zeros of a function inside a contour in the complex plane. The principle of the solution is based on those of the analytic functions without branch points, which is well known (Davies, 1986). The originality of the method used in our study is to take into account the double-valued property of the square root functions, present in the equation of dispersion (Cristini, 1994). This method allowed us to determine the zeros of equation (56), which had branch points $K_1^* = \pm k_m(1 + \frac{1}{2}\mathrm{i}\,\omega\nu_m)$ and $K_1^* = \pm k_0$, arising from the square root functions K_{L2}^*, K_{T2}^*, K_{F2}^*. The zeros of the function are indirectly defined by the arguments principle. The latter allows us to calculate the coefficients of a polynomial, which has the same roots as the function. The choice of the intergration contour was a circle.

For solving an equation with branch points, it is necessary to study the behavior of the square root functions in the complex plane, in order to understand correctly the problems. The difficulties of the solution came from the functions K_{L2}^*, K_{T2}^*, K_{F2}^*. Using double-valued functions implies to choose their value by defining a branch cut in the complex plane K_1^*. A good choice is to consider for example a criterion on the real or on the imaginary part. The advantage of these two definitions is that the two associated branch cuts have the same support (Figure 3). Thus, according to the region of the complex plane where one seeks the zeros, one chooses the appropriate branch cut. It has not to cross the chosen domain. Then one takes a close look at the two values of the square root functions.

For the solution of equation (56), the "imaginary part" criterion was chosen for each square root function $\boldsymbol{K}_{L2}^*$, $\boldsymbol{K}_{T2}^*$ and $\boldsymbol{K}_{F2}^*$:

$$\Im m\{\boldsymbol{K}_{L2}^*, \boldsymbol{K}_{T2}^*\} < 0, \quad (61)$$

$$\Im m\{\boldsymbol{K}_{F2}^*\} > 0. \quad (62)$$

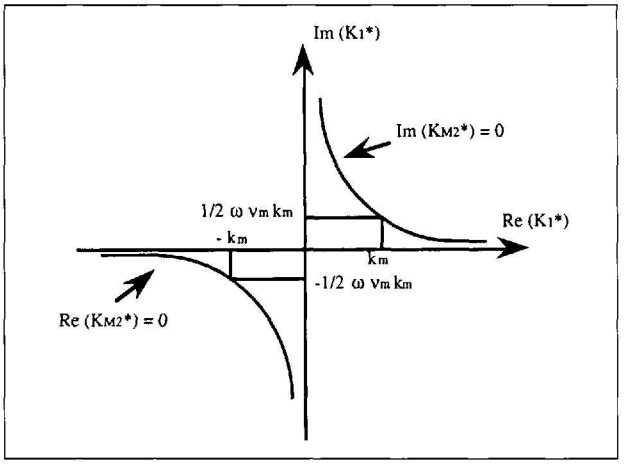

Figure 3. Representation of the branch cuts of the square root function K_{M2}^* in the complex plane K_1^*.

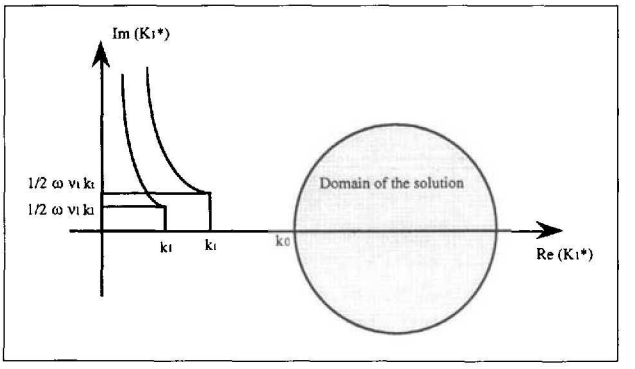

Figure 4. Representation of the domain of the solution to the equation of the dispersion of the Stoneley-Scholte wave (water/B2900 interface). (The branch cuts of all the square root function are shown.)

These criterions express the finite energy in both media. The solution to equation (60) has also verified these inequalities. And the wave vector of the Stoneley-Scholte wave verifies the inequality:

$$\Re e\{K_1^*\} > \max(k_0, k_t, k_l). \quad (63)$$

The domain of the complex plane, where the solution to equation (56) was seeked, is shown on Figure 4.

4.3. Numerical application: the water/B2900 and the water/PVC interfaces

The ideal fluid was represented by water and the viscoelastic solid by B2900 (a synthetic resin modelling limestone) loaded with alumina and tungsten ($c_t > c_0$), then by PVC ($c_t < c_0$). The acoustical characteristics of the media, assumed as constants in the frequency range 20 kHz–1 MHz, are summarized in Table II. The homogeneous wave attenuations of the solid increase with frequency. For the frequency 500 kHz, the longitudinal wave attenuations were equal to 110 dB/m for B2900 and to 130 dB/m for PVC, and the shear wave attenuations to 180 dB/m for B2900 and to 490 dB/m for PVC.

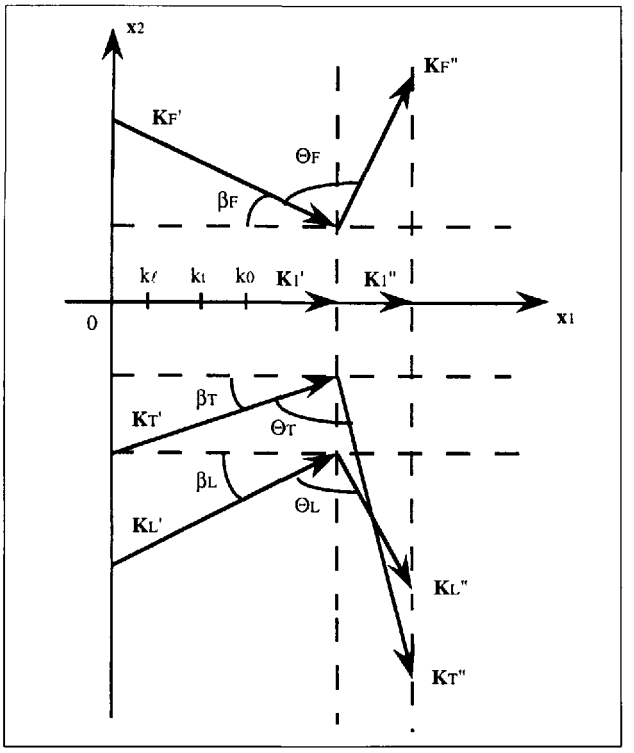

Figure 5. Representation of the problem of the Stoneley-Scholte wave at the water/B2900 interface, for the damped case. (The representation of the problem at the water/PVC interface is similar.)

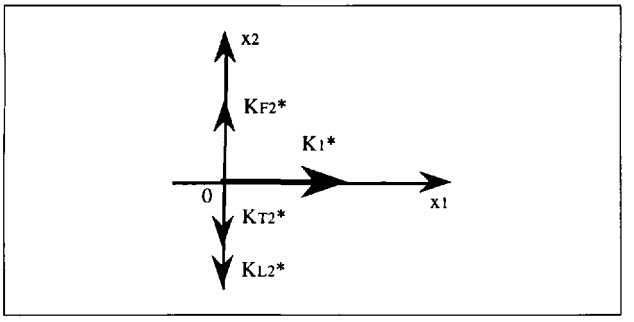

Figure 6. Representation of the problem of the Stoneley-Scholte wave at the water/B2900 interface, for the undamped case. (The representation of the problem at the water/PVC interface is similar.)

Table II. Some measured characteristics of the fluid (water) and the solids (B2900 and PVC).

Frequencies 20 kHz–1 MHz	Water	B2900	PVC
Density [kg/m^3]	1000	2000	1360
LW velocity [m/s]	1478	2910	2268
SW velocity [m/s]	—	1620	1100

The numerical solution to equation (56), for the frequency 60 kHz, gave the results of Table III, which led to those summarized in Table IV. The vector $\boldsymbol{K}'_M$ made an angle β_M

Table III. Theoretical results about the projection of the different wave vectors upon the axes and the velocity of the interface wave (frequency 60 kHz) (the results concerning the undamped case are written in italics).

Frequency 60 kHz	B2900	PVC
$\boldsymbol{K}^*_{L2}$ [1/m]	4 – 268 i *– 268 i*	9 – 391 i *– 392 i*
$\boldsymbol{K}^*_{T2}$ [1/m]	3 – 186 i *– 185 i*	7 – 251 i *– 252 i*
$\boldsymbol{K}^*_{F2}$ [1/m]	– 13 + 154 i *158 i*	– 14 + 340 i *341 i*
$\boldsymbol{K}^*_1$ [1/m]	298 + 7 i *298*	425 + 11 i *426*
c_{sch} [m/s]	1266 *1267*	887 *886*

Table IV. Theoretical characteristics of the inhomogeneous waves in both media (frequency 60 kHz) (the results concerning the undamped case are written in italics).

Frequency 60 kHz	Norm of $\boldsymbol{K}'_M$ [1/m]	Norm of $\boldsymbol{K}''_M$ [1/m]	Angle Θ_M [°]	Angle β_M [°]
Water lamel. w.	298 *298*	154 *158*	90 *90*	2.5 *0*
B2900 lamel. w.	298 *298*	268 *268*	89.4 *90*	0.8 *0*
B2900 tors. w.	298 *298*	186 *185*	88.5 *90*	0.5 *0*
Water lamel. w.	425 *426*	340 *341*	90 *90*	2 *0*
PVC lamel. w.	425 *426*	391 *392*	89.6 *90*	1.3 *0*
PVC tors. w.	425 *426*	251 *252*	88.3 *90*	1 *0*

with the axis (x_1):

$$\cos\beta_M = \frac{K'_1}{K'_M}. \tag{64}$$

The velocity c_{sch} of the Stoneley-Scholte wave was defined by:

$$c_{sch} = \frac{\omega}{K'_1}. \tag{65}$$

Thus, the problem of the Stoneley-Scholte wave could be represented as a combination of one evanescent wave in the fluid and two heterogeneous waves in the solid (Figure 5).

Note:

The results for the undamped case are expressed in the tables in italics. We can notice that the results concerning the two cases are not very different. Nevertheless, taking into account the attenuations in the solid is important, because the attenuation of the interface wave during its propagation is then known.

ACUSTICA · acta acustica
Vol. 82 (1996)

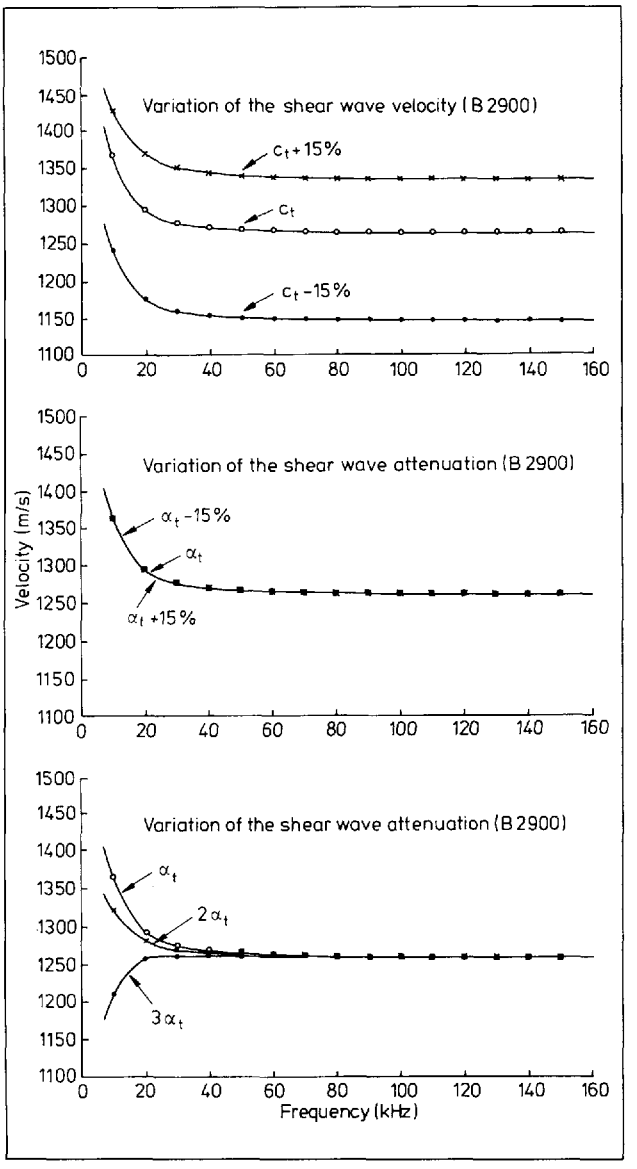

Figure 7. Theoretical effect of the shear wave attenuation and velocity of the solid on the dispersion curves of the Stoneley-Scholte wave (water/B2900 interface).

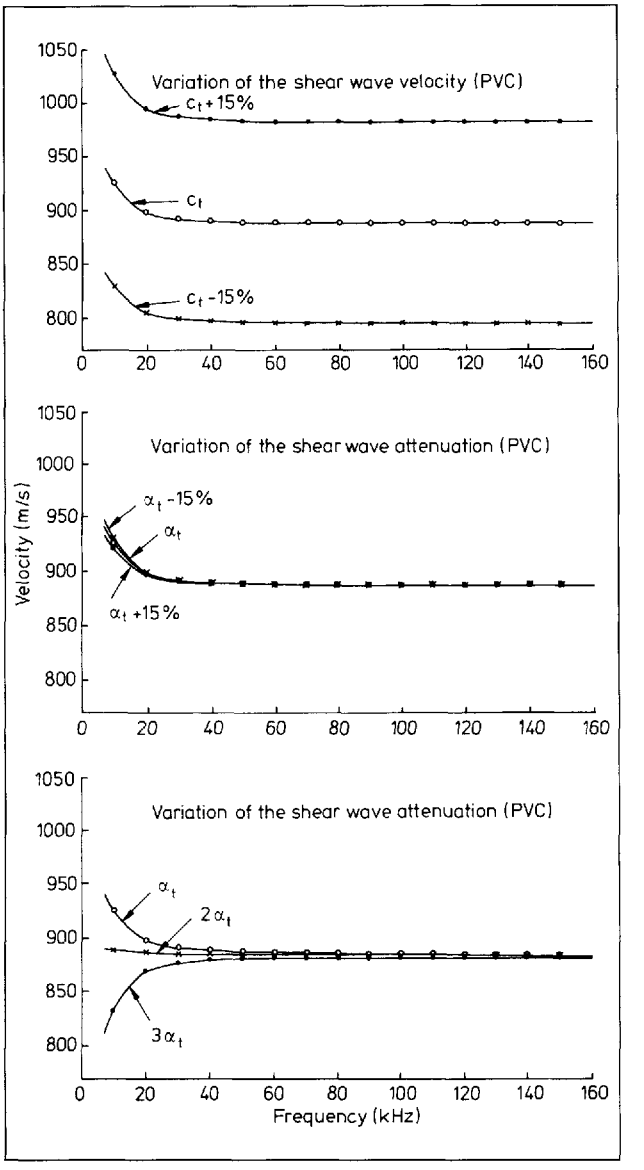

Figure 8. Theoretical effect of the shear wave attenuation and velocity of the solid on the dispersion curves of the Stoneley-Scholte wave (water/PVC interface).

The configuration of the problem of the Stoneley-Scholte wave at the ideal fluid/solid interface could be represented as a combination of three evanescent plane waves (Luppé, 1987) (Figure 6).

4.4. Effect of the shear wave attenuation and velocity in the solid on the dispersion curves of the interface wave

The dispersion curves of the "phase velocity" (Figures 7,8) correspond to increase and decrease of the parameters by 15%, in comparison with the real values given in Table II. The effects of the shear wave attenuation with increases of 100% and 200%, in comparison with the real values, are also shown.

In both cases (the water/B2900 and the water/PVC interfaces), the shear wave velocity was the parameter which most modified the dispersion curves. The variation of the curve values was approximately equal to 10%. Thus the shear wave velocity could be estimated with precision by means of the solution of the inverse problem. On the contrary, we would have great difficulty on estimating the shear wave attenuation in the solid with precision, even in the low frequency domain.

4.5. Densities of energy

The density of energy W in both media was expressed by:

$$W(\omega) = \frac{1}{2}\Sigma_{ij}(\omega)E_{ij}(\omega), \tag{66}$$

where $\Sigma_{ij}(\omega)$ defined the stress tensor components exerted on the solid, and $E_{ij}(\omega)$ the strain tensor components.

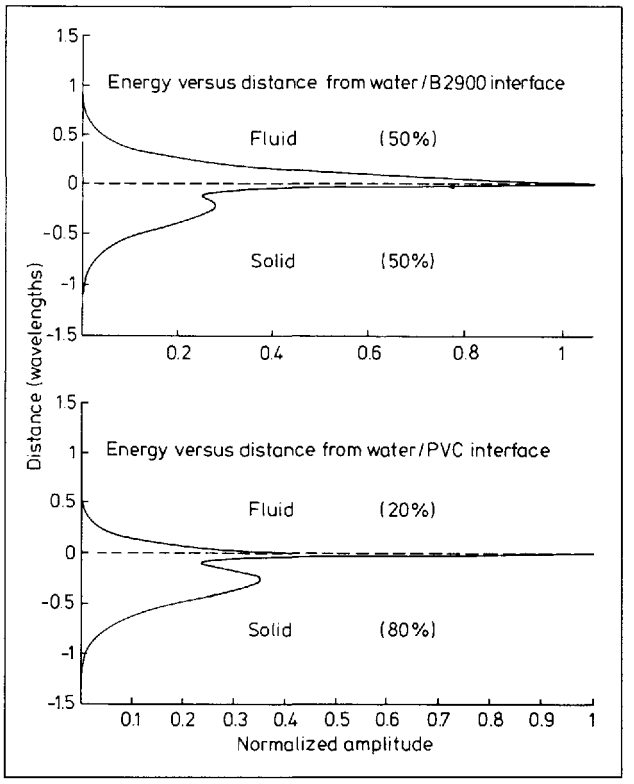

Figure 9. Theoretical distribution of the acoustical energy as a function of the distance from the interface (frequency 60 kHz, wavelengths λ =2.1 cm (B2900) and λ =1.5 cm (PVC), distance of propagation 20 cm, normalization of energy with the energy in the solid at the interface).

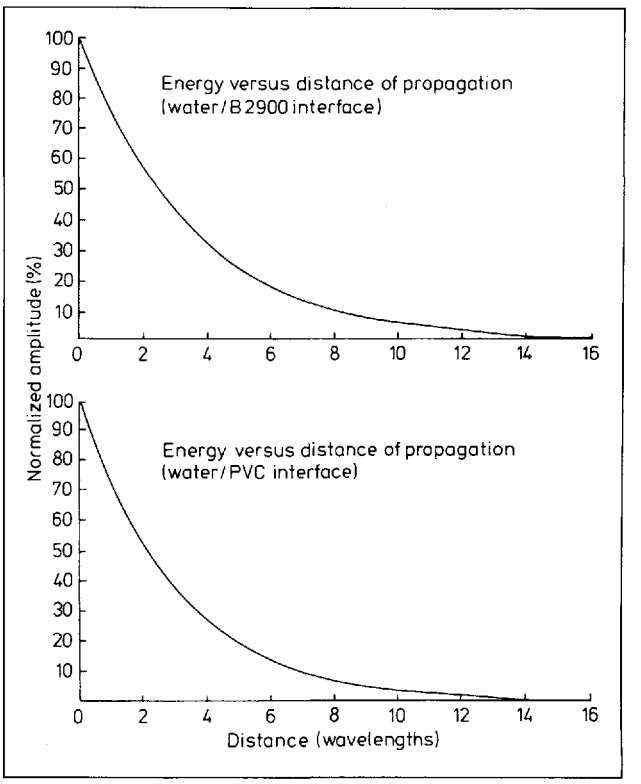

Figure 10. Theoretical attenuation of the energy of the Stoneley-Scholte wave during its propagation at the interface (frequency 60 kHz, wavelengths λ =2.1 cm (B2900) and λ =1.5 cm (PVC), normalization of energy with the enery near the source).

In the case of the isotropic viscoelastic solid, the stress tensor was given by the Fourier transforms of equations (1), (2) and (3):

$$\Sigma(\omega) = 2M(\omega)E(\omega) + \Lambda(\omega)\big(Tr\,E(\omega)\big)\boldsymbol{I} - 2\mathrm{i}\omega M'(\omega)E(\omega) - \mathrm{i}\omega\Lambda'(\omega)\big(Tr\,E(\omega)\big)\boldsymbol{I}, \tag{67}$$

where $M(\omega)$, $\Lambda(\omega)$, $M'(\omega)$, $\Lambda'(\omega)$ were the Fourier transforms of the Lamé coefficients and the viscosity coefficients.

In the ideal fluid, the Lamé coefficient M is equal to zero and:

$$\Sigma(\omega) = \Lambda_0\big(Tr\,E(\omega)\big)\boldsymbol{I}. \tag{68}$$

The strain tensor E was expressed in terms of displacements:

$$E = \frac{1}{2}\big(\mathrm{grad}\,\zeta + (\mathrm{grad}\,\zeta)^t\big). \tag{69}$$

The distribution of the acoustical energy in both media as a function of the distance from the interface showed that energy was concentrated in the solid and did not penetrate deep into both media (Figure 9). Moreover, the energy of the Stoneley-Scholte wave was quickly attenuated during its propagation at the interface (Figure 10). Therefore, we had difficulty in detecting the interface wave at the water/B2900 interface or at the water/PVC interface, and in general at the surface of the viscoelastic solids, which could model sediments.

5. The Stonely-Scholte wave at the plane interface between an ideal fluid and a viscoelastic solid-some experimental results

However, the Stoneley-Scholte wave could be excited at the surface of viscoelastic solids, and in particular at the boundary between water and PVC. It was generated with a shear wave transducer (resonance frequency: 100 kHz), associated with a solid wedge, and detected with a small transducer with a large band width, near the surface of the solid material. The first results obtained with this experimental set up were in good agreement with the theoretical and numerical ones: a wave with a similar velocity (difference between the theoretical and experimental velocities less than 3%) was detected. In particular, it verified the theoretical exponential decreases during its propagation along the interface (Figure 11) and far from the interface in the fluid (Figure 12). For the moment, some treatments are done for determining the properties of the Stoneley-Scholte wave at the water/B2900 interface.

6. Conclusion

The propagation of the Stoneley-Scholte wave, at the interface between in ideal fluid and a viscoelastic solid, has been investigated using the theory of the inhomogeneous plane waves. At first, the solid behavior has been introduced in the equation of propagation. A relation has been established

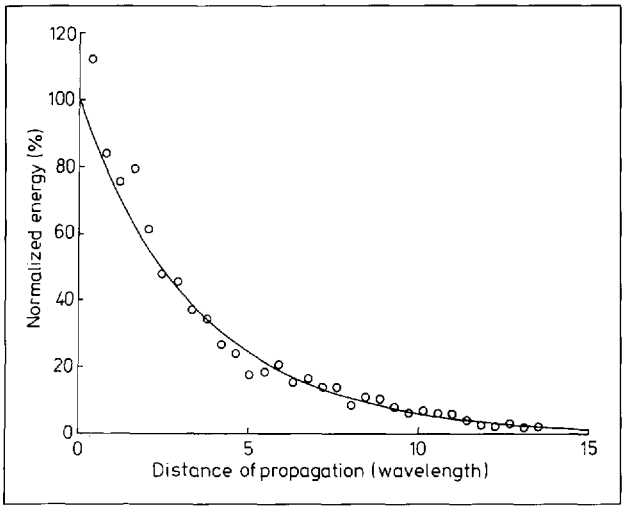

Figure 11. Comparison between theoretical (——) and experimental (o o) results: attenuation of the energy of the Stoneley-Scholte wave during its propagation at the water/PVC interface (frequency 75 kHz, wavelength $\lambda = 1.2$ cm, normalization of energy with the energy obtained for the first position of the receiver (3 cm from the source)).

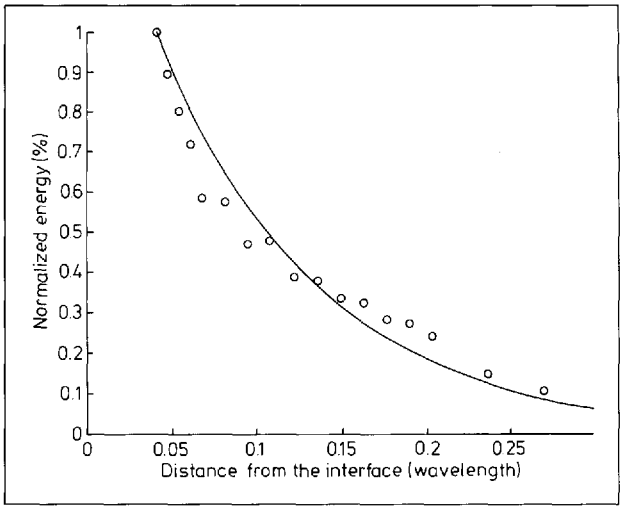

Figure 12. Comparison between theoretical (——) and experimantal (o o) results: attenuation of the energy of the Stoneley-Scholte wave far from the water/PVC interface (frequency 60 kHz, wavelength $\lambda = 1.5$ cm, normalization of energy with the energy obtained for the first position of the receiver (0,6 mm from the interface and 2 cm from the source)).

between the viscosity coefficients, which could not be determined by means of mechanical experiments in the high frequency range, and the acoustical attenuations in the solid, easily determined by means of acoustical experiments. Subsequently, the interface wave has been regarded as a linear combination of one evanescent wave in the fluid and two heterogeneous waves in the solid. Then, several properties concerning the interface wave have been determined, in particular about the distribution of energy in both media, and about the attenuation of the energy of the interface wave during its propagation. The effect of the shear wave attenuation in the solid material, in particular on the dispersion curves of the interface wave, has been shown. Finally, some experiments have been performed and the obtained results have been satisfactory. We have detected the Stoneley-Scholte wave at the water/synthetic resins interfaces and its properties have been in good agreement with the theoretical and numerical ones. Some other experiments concerning the propagation of the interface wave and theoretical study of the inverse problem, that is determining the shear wave characteristics by means of those of the interface wave, are now under consideration.

Acknowledgement

The author would like to thank Dr. J.-P. Sessarego, Dr. B. Poirée, Dr. P. Cristini and Dr. G. Rabau for their help with this work.

References

Bjørnø, L., Papadakis, J. S., Papadakis, P. J., Sagéloli, J., Sessarego, J.-P., Sun, S., and Taroudakis, M. I. (1994). Identification of seabed data from acoustic reflections: theory and experiment. *Acta Acustica* **2**, 359–374.

Caiti, A., Akal, T., and Stoll, R. D. (1991). Determination of shear velocity profiles by inversion of interface wave data. *Shear Waves in Marine Sediments*, 557–566.

Chapman, R., Levys, S., Cabrera, J., Stinson, K., and Oldenburg, D. (1986). The estimation of the density P-wave and S-wave speeds of the top most layer of sediments, from water bottom reflection arrivals. Akal, T. and Berkson, J. M., editors, *Ocean Seismo-Acoustics*, Plenum Press, New York, 703–710.

Cristini, P. (1994). Calcul des zéros d'une fonction analytique avec points de branchements. *Journal de Physique* **IV**, 869–872. Colloque C5, supplément au *Journal de Physique* III 4.

Davies, B. (1986). Locating the zeros of an analytic function. *Journal of computational physics* **66**, 36–49.

Deschamps, M. (1991). L'onde plane hétérogène et ses applications en acoustique linéaire. *Journal d'Acoustique* **4**, 269–305.

Ewing, W. M., Jardetsky, W. S., and Press, F. (1957). *Elastic waves in layered media*. Mac Graw Hill, New York.

Guilbot, J. (1994). *Caractérisation acoustique de fonds sédimentaires marins par étude de la dispersion de célérité des ondes d'interface de type Stoneley-Scholte*. PhD thesis, INSA, Lyon.

Jensen, F. B. and Schmidt, H. (1986). Shear properties of ocean sediments determined from numerical modelling of Scholte wave data. Akal, T. and Berkson, J. M., editors, *Ocean Seismo-Acoustics*, Plenum Press, New York, 683–692.

Le Tirant, P. (1976). *Reconnaissance des sols en mer pour l'implantation des ouvrages pétroliers*. Ed. Technip.

Lemaître, J. and Chaboche, J.-L. (1985). *Mécanique de matériaux solides*. Dunod, Paris.

Luppé, F. (1987). Contribution à l'étude de l'onde de Scholte-Stoneley à différentes interfaces fluide parfait/solide élastique. Master's thesis, Sciences Physiques, Université Paris VII, France.

Poirée, B. (1989). Les ondes planes évanescentes dans les fluides et les solides élastiques. *Journal d'Acoustique* **2**, 205–216.

Poirée, B. (1991). Complex harmonic plane waves. Leroy, O. and Breazeale, M. A., editors, *Physical Acoustics*, Plenum Press, New York.

Poirée, B. and Luppé, F. (1991). Evanescent plane waves and the Scholte-Stoneley interface waves. *Journal d'Acoustique* **4**, 575–588.

Rabau, G. (1990). *Modèles géoacoustiques*. PhD thesis, Université d'Aix-Marseille II, France.

Salençon, J. (1983). *Viscoélasticité*. Presses Ecole Nationale des Ponts et Chaussées, Paris.

Vol'kenshtein, M. M. and Levin, V. M. (1988). Structure of a Stoneley wave at an interface between a viscous fluid and a solid. *Sov. Phys. Acoust.* **34(4)**, 351–355.